Sensitivity Analysis of GaSb/GaAs Type-II Heterojunction STFET as a Dielectric Modulated Label-Free Biosensor

7.1 Introduction

Various types of field effect transistor (FET) based biosensors such as the ISFET (ion sensitive field-effect transistor) and DMFET (dielectric modulated field effect transistor) have been explored due to their compatibility with wide ranges of biomolecules and flexibility for on-chip integration using well matured CMOS technology [235]. The major drawback of the ISFET based biosensors is ineffective to determine the presence of neutral biomolecules. The bulk MOSFET (metal– oxide–semiconductor field-effect transistor) structure based DMFET biosensors have been used to sense many types of biomolecules [215], [235]-[237]. Several researchers have explored the tunnel FET (TFET) structure for label-free biosensing applications [214]-[217]. Therefore in chapter-6, we have designed backgated ferroelectric TFET on SELBOX substrate (BG-Fe-HJ-STFET) based biosensor. Low band gap material germanium (Ge) has been used for the designing of BG-Fe-HJ-STFET based biosensor because the use of a gate/source heterojunction with a low bandgap material for the source is a common technique to enhance the drain current of the TFETs [174], [238]. III-V based semiconductor like GaAs [231], InAs [105] and GaSb [239] materials have been shown to further improve the drain current significantly than IV-IV used in previous chapters due to their higher mobility. Therefore in in this chapter we have used low bandgap GaSb in place of germanium and GaAS in place of Si. Further unlike chapter-5 and 6 back gate is not used here because back gate increases drive current at cost of increased ambipolarity which is undesired as discussed in chapter-5. III-V semiconductor itself increases the drive current

due to higher mobility than IV-IV. Therefore we have used here III-V based semiconductor heterojunction in place of IV-IV based heterojunction. This chapter explores a GaSb/GaAs type-II heterojunction based TFET with SiO_2/HfO_2 vertically stacked gate-oxide for the label-free biosensing applications.

Different biomolecules such as uricase, ChOX, APTES, protein (streptavidin), biotin, HEWL, tranquilizer, DNA, Keratin, and protein have different dielectric constants ranging from 3 to 12 [220]-[222]. Since all the biomolecules have their own dielectric constants value, the dielectric constant of the FET is modulated according to the biomolecules thereby changing the drain current and threshold voltage of the DMFETs [219]-[235]. This type of sensing phenomenon is known as label-free detection of biomolecules [235]. Kanungo *et al*. [242] has reported a TFET biosensor using a SiGe as N^+ pocket at source/channel junction to improve its subthreshold current of the device. A dielectric modulation based electrically doped TFET (DM-ED-TFET) biosensor with an I_{ON}/I_{OFF} ratio of 10^{10} and current sensitivity of 10^8 has been investigated by Venkatesh *et al*. [243]. M. Verma *et al*. [244] have used an n+ source-pocket in a vertical DMTFET (V-DMTFET) based biosensor to achieve the channel current sensitivity of 10^2 and I_{ON}/I_{OFF} of 10^9 for biomolecules with dielectric constant k = 4. Chakraborty *et al*. [230] investigated a staggered heterojunction-based TFET biosensor to demonstrate its drain current sensitivity of $7.5x10^8$. However, the sensitivity values discussed above are not good enough to qualify for a good biosensor. Present chapter deals with GaSb/GaAs heterojunction (HJ) TFET on SELBOX substrate based DMTFET biosensor with a vertically stacked SiO_2/HfO_2 gate- dielectric oxide. The proposed device is named as GaSb/GaAs HJ-TFET. The sensing performance parameters of dual cavities (DC) at both the source and drain sides of the gate-oxide (we denote it as DC-HJ-STFET) have been investigated in the present study using the commercially available ATLAS^{TM} TCAD tool.

7.2 Device for Study

7.2.1 Device Structure

3-D cross sectional view of DC-HJ-STFET based biosensors is shown by Figure 7.1. The work function of gate material is assumed 4.2 eV. The thickness (t_s) of (p+ GaSb) source region is 15 nm with acceptor doping concentration of $1x10^{20}$ cm^{-3}. A p-GaAs channel with doping concentration of $1x10^{16}$ cm^{-3} andthickness ($t_{BODY} = t_s$) of 15 nm is used in the proposed "biosensors". The drain contact is made on the n^+ GaAs drain region with a doping concentration of 5×10^{18} cm^{-3}. Each cavity thickness (t_c) of 4 nm is used for the simulation. The compound semiconductor material parameters used for simulation of proposed DC-HJ-STFET based biosensor are listed in Table 7.1. Some significant biomolecules with dielectric constants whose size smaller than 4 nm are mentioned in Table 7.2. Table 7.3 shows the list of all the dimensional parameters of the proposed device.

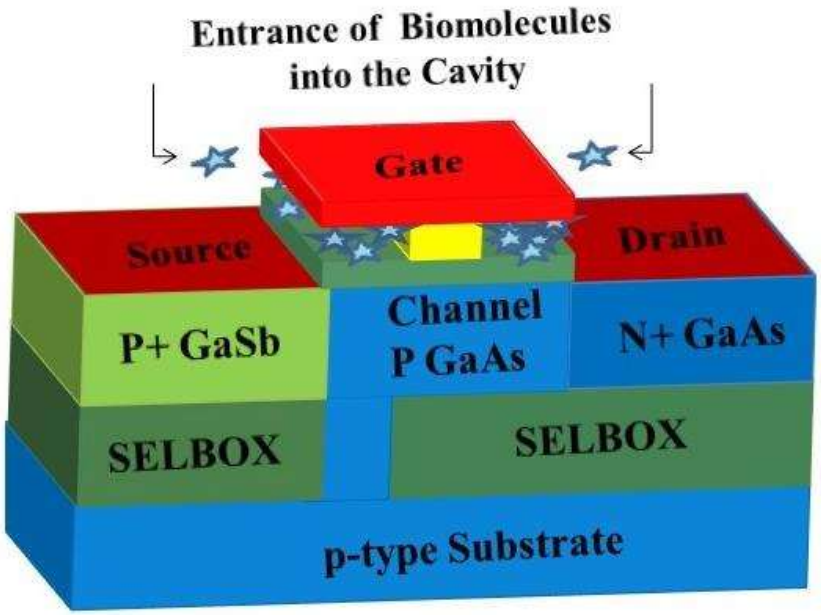

Figure 7.1 3D schematic structures of DC-HJ-STFET based biosensors.

Table 7.1 GaSb and GaAs Materials Parameters for theSimulation study [222], [245].

Materials	Electron Affinity (eV)	Light Hole mass	Effective Electron mass	Lattice Constant (A)	Energy gap, E_g (eV)
GaSb	4.06	0.40 m_o	0.041 m_o	6.096	0.67
GaAs	4.07	0.51 m_o	0.063 m_o	5.450	1.44

Table 7.2: Some important biomolecules with dielectric Constant value [222] [226], [228], [237]-[238].

Biomolecules	Dielectric Constant
Biotin	2.63
ChOx	3.3
GOx	3.46
APTES	3.57
DNA	6
Gelatin	12

7.2.2 Fabrication Process Flows and Models Validation

The proposed DC-HJ-STFET construction can be manufactured utilizing comparable steps as revealed in [109], [246]. The required fabrication process flows of the proposed DC-HJ-STFET are shown in Figure 7.2. In the first step of fabrication, we have to choose a clean p-type GaAs substrate on which the remaining fabrication process can be performed easily and deposited the buried oxide (BOX) SiO_2 layer over the selected substrate by using thermal oxidation process as shown in Figure 7.2 (a). In the next step the SELBOX gap is created by the etching of GaAs and the growth of the n+ GaSb and p− GaAs layers over the BOX layer by using the epitaxial method in the third step of the process flow as shown in Figure 7.2 (b). Then masking is pattern for the etching the GaAs the remaining part rather than channel and drain region then two cavities are made in

p−GaAs layer where the p+ GaSb and n+ GaAs are deposited by using CVD process as depicted by Figure 7.2 (c) to construct the source and channel regions of the device. After forming source and drain region, we have to dope it with required types of doping. In the succeeding advance, SiO_2/HfO_2 is kept as a gate oxide and then metallization and designing are done to acquire the source, drain and gate contacts then nanocavities are formed in HfO_2 on both side of the gate as illustrated in Figure 7.2 (d).

The performance of the proposed DC-HJ-STFET biosensor is analysed by using the commercially available TCAD tool (SILVACO ATLAS) [37]. The non-local band to band tunneling (BTBT), SRH, Auger recombination (AR), Shockley-Read-Hall (SRH) generation-recombination (GR), field-dependent mobility and Fermi-Dirac statistics models have been used. Calibration of the TCAD tool has been carried out by contrasting the simulated drain current data and the prefabricated data for a SOI TFET as shown in Fig. 3 [38]. A reasonably good matching between the TCAD simulation and experimental data confirms the validity of the ATLAS TCAD tool to be used for the performance analysis of the proposed biosensors.

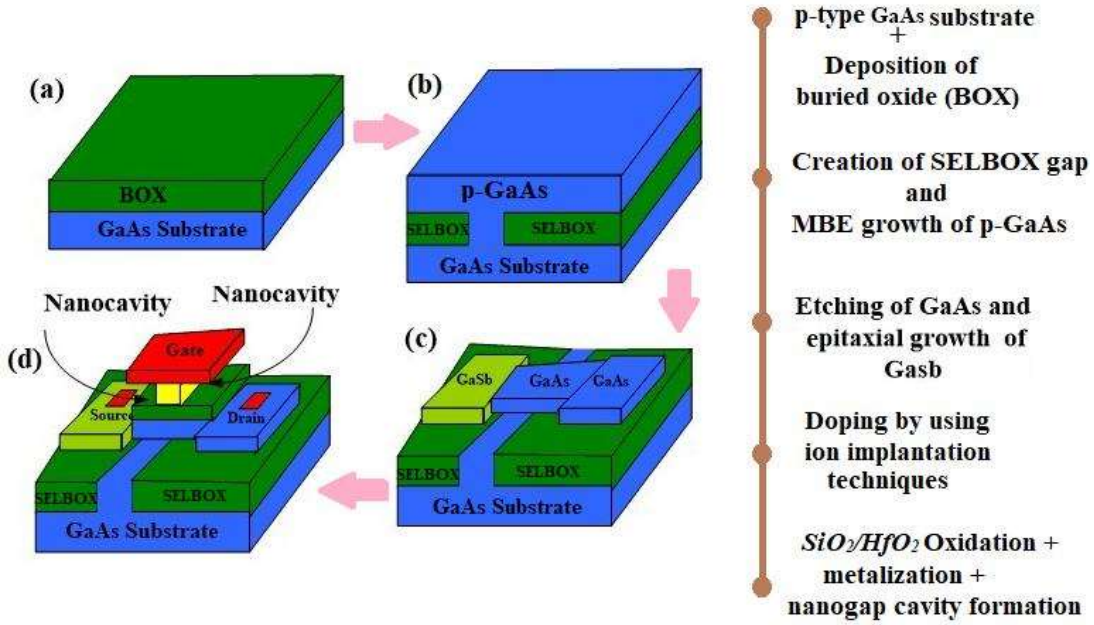

Figure 7.2 Fabrication Steps of DC-HJ-STFET biosensor.

Table 7.3: List of device's (DC-HJ-STFET) dimensions and structural parameters.

Parameters	**Value**	**Unit**
Source doping concentration (N_S)	1×10^{19} cm^{-3}	$1\times10^{19}cm^{-3}$
Channel doping concentration (N_{ch})	1×10^{16} cm^{-3}	1×10^{16} cm^{-3}
Drain doping concentration (N_D)	5×10^{18} cm^{-3}	5×10^{18} cm^{-3}
The thickness of the channel (t_{Si})	15 nm	15 nm
The thickness of SiO_2 gate oxide (t_{ox})	1 nm	1 nm
The thickness of High-k gate oxide (t_{ox})	2 nm	2 nm
Effective Oxide Thickness (EOT)	1.312 nm	1.312 nm
Gate length (L_G)	40 nm	40 nm
Source length (L_S)	30 nm	30 nm
Drain length (L_4)	30 nm	30 nm
Thickness of buried oxide (BOX) (t_{BOX})	10 nm	10 nm
Length of SELBOX gap (L_2)	2 nm	2 nm
Hole tunnel mass in silicon (m_{htSi})	$0.24m_o$	$0.24m_o$
Hole tunnel mass in germanium (m_{htGe})	$0.044m_o$	$0.044m_o$
Electron tunnel mass in silicon (m_{etSi})	$0.20m_o$	$0.20m_o$
Electron tunnel mass in germanium (m_{etGe})	0.082mo	0.044mo
Lattice constant of Ge	5.656 ^{0}A	5.656 ^{0}A
Lattice constant of Si	5.429 ^{0}A	5.429 ^{0}A
Bandgap energy Ge	0.70 eV	0.70 eV
Bandgap energy Si	1.12 eV	1.12 eV
Electron affinity Ge	4.01 eV	4.01 eV
Electron affinity Si	4.05 eV	4.05 eV
Dielectric Constant of ferroelectric material	1495	------
Front Gate Metal Work Function (eV), ψ_{sf}	4.1 eV	4.1 eV
Back Gate Work Function (eV), ψ_{sb}	4.1 eV	4.1 eV

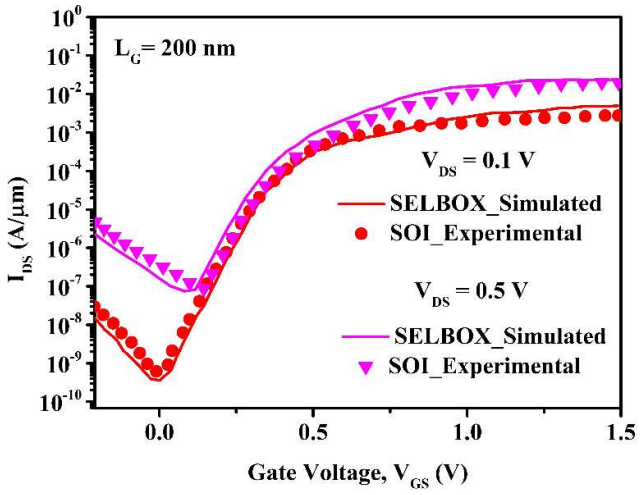

Figure 7.3 Calibration of the ATLAS TCAD tool by comparing the simulated drain current with experimental data of an SOI TFET reported in [158].

7.3 Results and Discussion

This section presents some electrostatic analyses for the proposed DC-HJ-STFET biosensors. Firstly, we have considered both the positive and negatively charged biomolecules with dielectric constants k = 3, 5, 7, 10 and 12. Usually, the sensitivity is measured in terms of the variation of drain current, threshold voltage and subthreshold swing of the DMFET sensors [39]. Air is used as a reference dielectric for the calculation of all kinds of sensitivities. The sensitivity of a DMFET biosensor is given by [225]-[239]:

$$Sensitivity = \left. \frac{I_d^{Bio} - I_d^{Air}}{I_d^{Air}} \right|_{V_{GS}, V_{DS}} \tag{7.1}$$

where, I_d^{Bio} and I_d^{Air} are the drain currents with biomolecules (with dielectric constant k > 1), and without of biomolecules (i.e., with air with k = 1), respectively, at fixed V_{GS} and V_{DS}.

7.3.1 Analytical Modeling of Surface Potential

The potential distribution in the gate oxide and channel region of the TFET is governed by 2-D Poisson's equation [147]. The 2D schematic of HJ-STFET is shown in Figure 5.4

and it shows the entire region that considered while developing the analytical model (from R1 to R4). The following assumptions were made in developing the surface potential. In all regions, uniform doping concentration is taken into account. Gate current, fixed oxide charge, and interface trap are not taken into account in this proposed model.

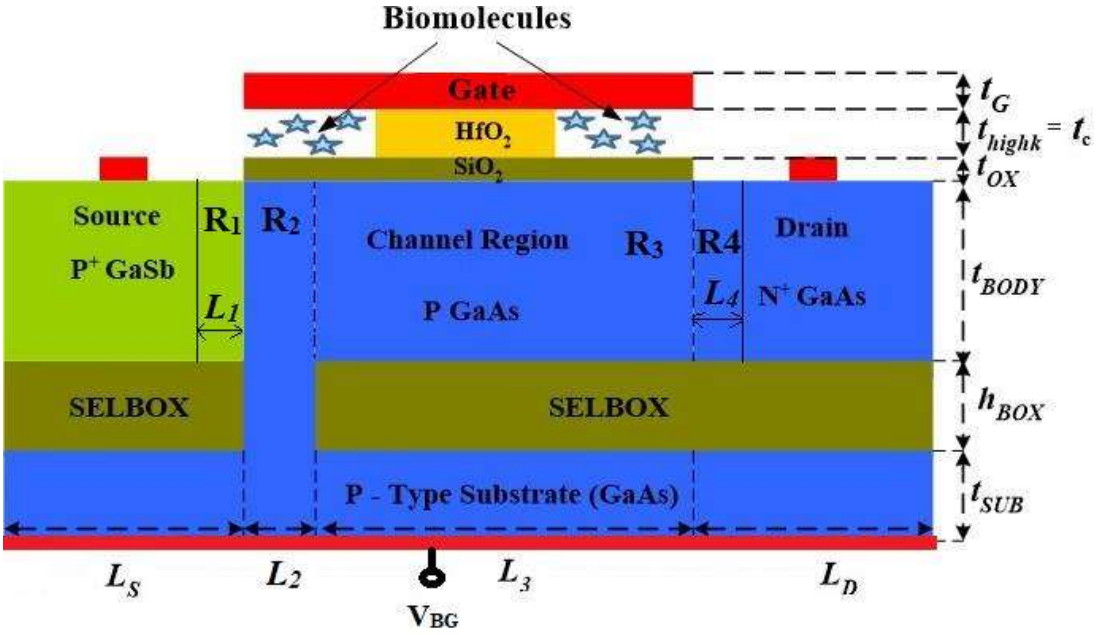

Figure 7.4 2D structure of DC-HJ-STFET based biosensors.

$$\frac{\partial^2\psi_i(x,y)}{\partial x^2}+\frac{\partial^2\psi_i(x,y)}{\partial y^2}=\frac{-qN_i}{\varepsilon_{si}} \qquad \text{for } i=1,\ 2,\ 3,\ 4 \tag{7.2}$$

Using the parabolic potential approximation, the 2-D channel potential function $\psi_i(x,y)$ in the region R_i (i=1,2,3,4) can be expressed as

$$\psi_i(x,y)=C_{0i}(x)+C_{1i}(x)y+C_{2i}(x)y^2 \tag{7.3}$$

where, $C_{0i}(x)$, $C_{1i}(x)$ and $C_{2i}(x)$ are arbitrary functions of x to be determined by using the following boundary conditions:

$$\psi_{is}(x)=C_{0i}(x)=\psi_i(x,y)\big|_{y=0} \tag{7.4}$$

Where $\psi_{is}(x)$ is the surface potential

$$\varepsilon_{Si}\left.\frac{d\psi_i(x,y)}{dy}\right|_{y=0}=\frac{\varepsilon_{ox}}{t_{ox}}\left(V_{GS}-V_{fb}-\psi_{is}(x)\right) \tag{7.5}$$

$$\varepsilon_{Si}\left.\frac{d\psi_i(x,y)}{dy}\right|_{y=t_{Si}}=\frac{\varepsilon_{ox}}{t_b}\left(V_{sub}-V_{ff}-\psi_i(x,t_{Si})\right) \tag{7.6}$$

For Region (i=1,3,4) and (i=2) we use (7.6)

$$\varepsilon_{Si}\left.\frac{d\psi_i(x,y)}{dy}\right|_{y=t_{Si}}=0 \tag{7.7}$$

$$V_{fb}=\phi_m-\chi_i+\frac{E_{gi}}{2}+V_{fi}$$

Where

$$V_{fi}=V_t\ln\left(\frac{N_i}{n_i}\right) \tag{7.8}$$

By solving Eq (7.2) to (7.8) we get

$$C_{1i}(x)=\frac{\varepsilon_{ox}}{t_{ox}\varepsilon_{Si}}\left(V_{GS}-V_{fb}-C_{0i}(x)\right) \tag{7.9}$$

$$C_{2i}(x)=\frac{\varepsilon_{ox}}{t_{ox}\varepsilon_{Si}}\left\{\frac{V_{G2}}{t_b}-\frac{V_{G1}}{t_{ox}}\left(1+\frac{\varepsilon_{ox}}{t_{ox}t_b}\right)+C_{0i}(x)\left[\frac{t_b-t_{ox}-\varepsilon_{ox}}{t_{ox}t_b}\right]\right\}$$

$$V_{G2}=V_{sub}-V_{ff} \tag{7.10}$$

$$V_{G1}=V_{GS}-V_{fb}$$

Putting (7.9) and (7.10) in (7.2) and applying (7.1) we get

$$\left.\frac{\partial^2\psi_i(x,y)}{\partial x^2}\right|_{y=0}+\left.\frac{\partial^2\psi_i(x,y)}{\partial y^2}\right|_{y=0}=\left.\frac{-qN_i}{\varepsilon_{si}}\right|_{y=0} \tag{7.11}$$

Solving (7.11) we get the following 1-D differential equation

$$\frac{d^2\psi_{is}(x)}{dx^2}+\frac{\psi_{is}(x)}{\lambda}=\frac{qN_i}{\varepsilon_{Si}}-P_i \tag{7.12}$$

$$p_i=-\lambda\frac{\left(\frac{\varepsilon_{ox}}{\varepsilon_{Si}t_{Si}}\left[\frac{V_{G2}}{t_b}-\frac{V_{G1}}{t_{ox}}\left(1+\frac{\varepsilon_{ox}}{t_{ox}t_b}\right)\right]\right)}{\left(1+\frac{\varepsilon_{ox}t_{ox}}{2\varepsilon_{Si}t_b}\right)} \tag{7.13}$$

$$\lambda = \left(1+\frac{\varepsilon_{ox}t_{Si}}{2\varepsilon_{Si}t_b}\right) \Big/ \left(\frac{t_b - t_{ox} - \varepsilon_{ox}}{t_b - t_{ox}}\right) \tag{7.14}$$

$$\psi_i(x,y) = K_{1i}\exp\left(\sqrt{\frac{1}{\lambda}}(x-x_{i-1})\right) - K_{2i}\exp\left(-\sqrt{\frac{1}{\lambda}}(x-x_{i-1})\right) \tag{7.15}$$

The value of K_{1i} and K_{2i} are obtained by solving the following boundary conditions

$$\psi_0 = \psi_1(0,y) = -V_T\ln(N_1/n_i) \tag{7.16}$$

$$\psi_1 = \psi_2(L_1,y) \tag{7.17}$$

$$\psi_3 = \psi_2(L_1+L_2,y) \tag{7.18}$$

$$\psi_4 = \psi_3(L_1+L_2+L_3,y) \tag{7.19}$$

$$\psi_4(L_1+L_2+L_3+L_4,y) = V_T\ln(N_4/n_i) + V_{DS} \tag{7.20}$$

$$\left.\frac{\partial\psi_{s,i}}{\partial x}\right|_{x=x_i} = \left.\frac{\partial\psi_{s,(i+1)}}{\partial x}\right|_{x=x_i} \quad \text{at } x=x_i \quad (i=1,2,3) \tag{7.21}$$

From boundary conditions (7.16)-(7.21) the values of constant K_1 and K_2 are obtained as

$$K_{1i} = \frac{-1}{2\sinh(\sqrt{\frac{1}{\lambda}}_i L_i)}\left(\psi_{i-1}\exp(-\sqrt{\frac{1}{\lambda}}_i L_i) - P_i(1+\exp(-\sqrt{\frac{1}{\lambda}}_i L_i)) - \psi_i\right) \tag{7.22}$$

$$K_{2i} = \frac{1}{2\sinh(\sqrt{\frac{1}{\lambda}}_i L_i)}\left(\psi_{i-1}\exp(\sqrt{\frac{1}{\lambda}}_i L_i) - P_i(1+\exp(\sqrt{\frac{1}{\lambda}}_i L_i)) - \psi_i\right) \tag{7.23}$$

The variation of surface potential in the device for different dielectric constant values of the biomolecules is illustrated in Figure 7.5. Where symbols represents the TCAD based simulation data and lines represents the model data.

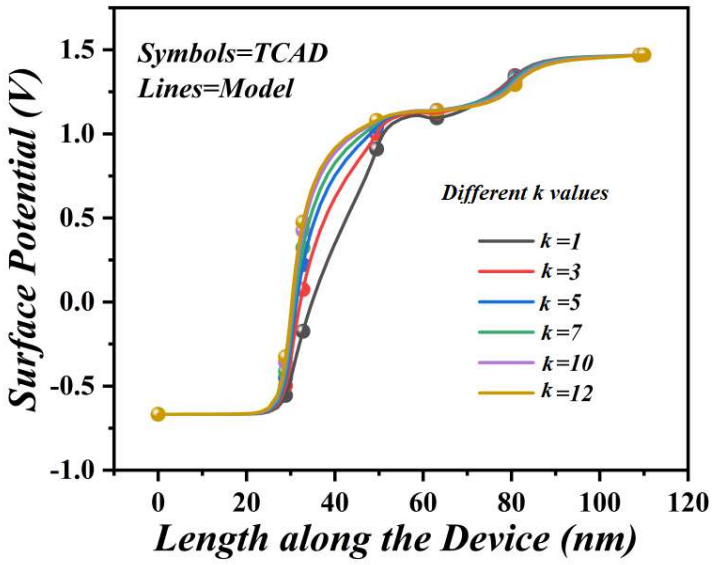

Figure 7.5 The surface potential plots along the length of the device at V_{DS} = 1.0 V, V_{GS} =1.0 V for different dielectric constant of the biomolecules.

7.3.2 Electrostatic Analysis Using Neutral Charge Biomolecules

The basic working operation of TFETs is based on band-to-band tunneling (BTBT) phenomenon. The drain current (I_{DS}) of TFETs can be calculated by integration band-to-band tunneling (BBT) generation rate (G) over the channel region. [99]:

$$I_{DS} = qW_{CH}\int Gdxdy \tag{7.24}$$

where W_{CH} means the channel width and G is the BTBT rate,

G can express as [99].

$$G_{BTBT} = AE^{\sigma}\exp\left(-\frac{B}{E}\right) \tag{7.25}$$

where A is a constant related to the effective mass of the electron ($4x10^{14}$ $V^{-2}s^{-1}cm^{-2}$), σ denotes the transition coefficient. E (MV/cm) magnitude of the local electric field and B is the tunneling probability constant (MV/cm).

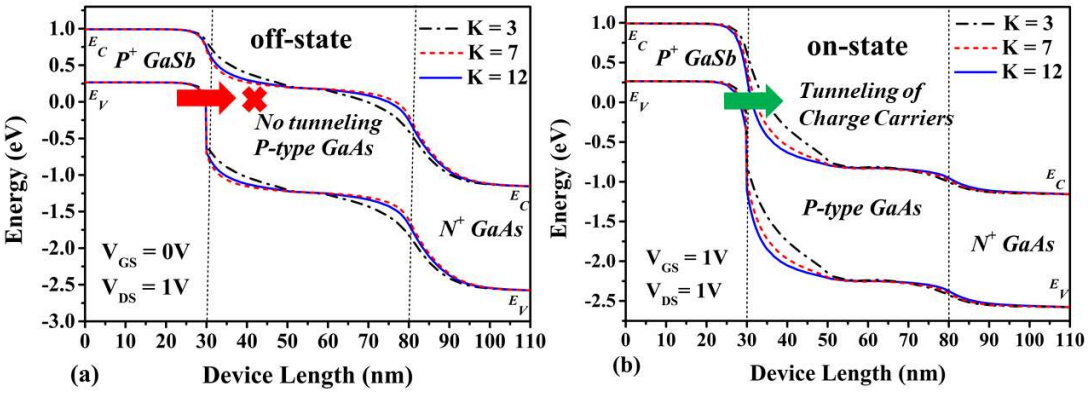

Figure 7.6 Plots of (a) OFF-state and (b) ON-state energy band diagram of DC-HJ-STFET based biosensor for k = 3, 7 & 12 at t_C = 4nm.

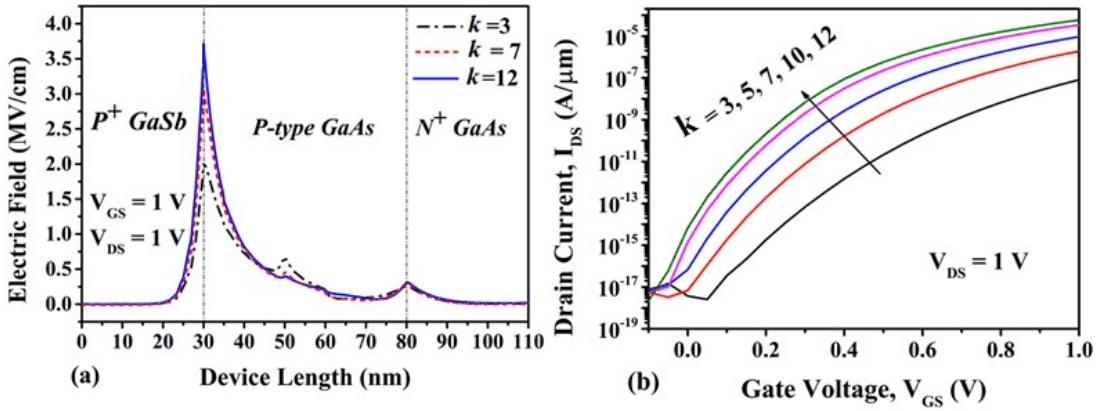

Figure 7.7 Plots of (a) 2-D Electric field and (b) drain current of DC-HJ-STFET based biosensor for k = 3, k = 7 & 12 at t_C = 4nm.

In order to understand the basic tunneling phenomenon of the proposed structures, the energy band diagrams in off- state and on-state of the proposed structure have been shown in Figure 7.6 for k = 3, k = 7 and k= 12. It is clear from Figure 7.6 (b) that for k = 3, there is less overlapping between valence band and conduction band whereas the overlapping increases significantly for k = 7 and k = 12. Thus, higher dielectric constant-based biomolecules cause larger overlapping between the valance band of source and conduction band of channel thereby increasing the tunnelling probability TWKB of carriers from the source to the channel of the TFET. Biomolecules with higher k values result in higher electric fields in the channel of the proposed TFET structure as

demonstrated in Figure 7.7 (a). Figurre 7.7 (b) shows the I-V characteristics of the proposed biosensor in the presence of different biomolecules with different dielectric constant value. It can be clearly understood from aforesaid figures that the higher *k* values leads to higher ON-state current.

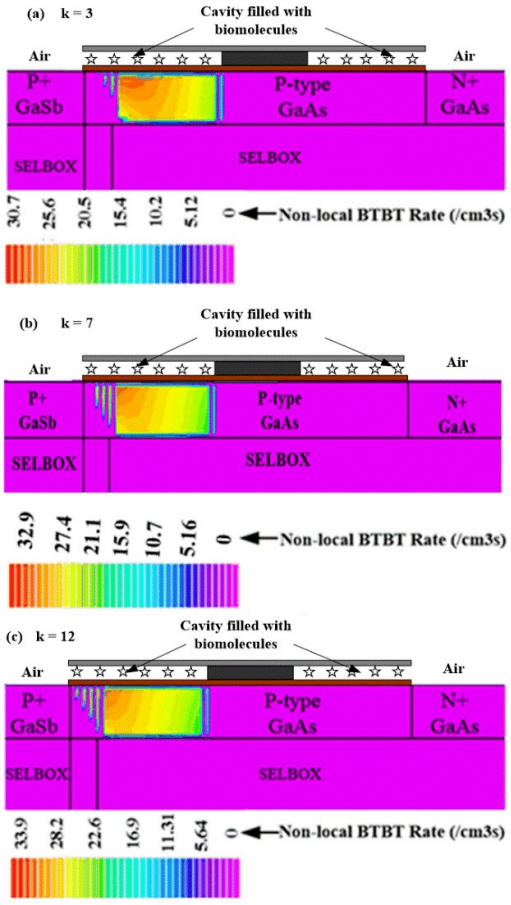

Figure 7.8 2-D non-local band to band tunnelling (BTBT) contour DC-HJ-STFET based biosensor for (a) k = 3, (b) k = 7, & (c) k = 12 at V_{GS} = 1V, V_{DS} = 1V and t_c = 4 nm.

Figure 7.8 (a, b and c) shows the 2-D non-local BTBT contour plots of the proposed sensors for k=3, k=7 and k=12 respectively. From the Figure 7.8 (a, b and c) it can be understood that the higher the k value, higher the BTBT rate for the DC-HJ-STFET structure. The reason for the same can be attributed to increase in electric field with increase in k values. The effect of dielectric modulation for different cavity thickness (t_c)

on (I_{ON} and I_{ON}/I_{OFF} sensitivity) and (threshold voltage (V_T) and threshold voltage sensitivity (S_{VT})) are shown in Figure 7.9 (a) and Figure 7.9 (b), respectively. The parasitic capacitance between source and channel reduces with the increment in cavity thickness, therefore the tunnelling width become larger at source and channel junction which results in the reduction of drain current [42], as illustrated in the Figure 7.9 (b) In Figure 7.9 (b), The threshold voltage and threshold voltage sensitivity increase as the cavity thickness increases, because when tunnelling width increases then turn on voltage (threshold voltage) automatically increases, therefore control of gate voltage on wider tunneling width reduces [222]-[230].

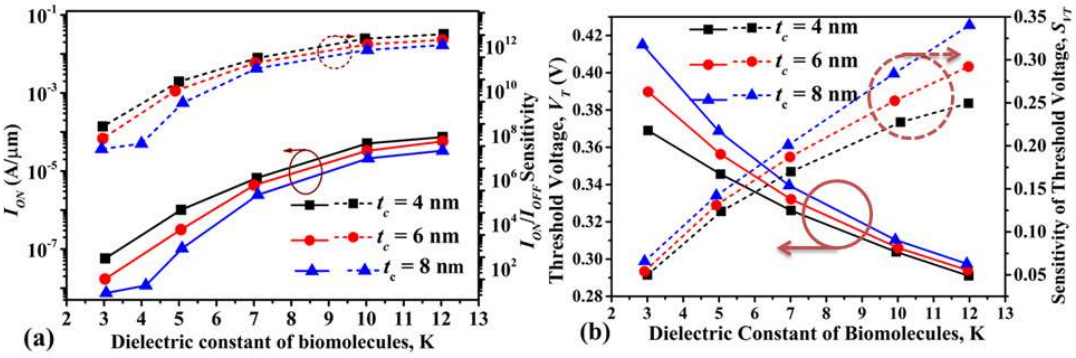

Figure 7.9 Plots of (a) I_{ON} and I_{ON}/I_{OFF} sensitivity and (b) threshold voltage (V_T) and threshold voltage sensitivity (S_{VT}) of DC-HJ-STFET based biosensor for different dielectric constant of biomolecules for different value of cavity thickness at V_{GS} = 1V, V_{DS} = 1V.

7.4.3 Impact of Negatively Charged Biomolecules

The I_{ON} current and I_{ON}/I_{OFF} sensitivities of DC-HJ-TFET biosensor with the cavities filled with negatively charged biomolecules for k = 3, 7, and 12 are shown in Figure 7.10 (a) whereas threshold voltage and threshold voltage sensitivity are shown in Figure 7.10 (b), respectively. The sensitivity is decreased with the increased magnitude of the negative charge of the biomolecules, whereas, the magnitude of I_{ON} is decreased and magnitude of threshold voltage is increased with the increased magnitude of the negative charge of the biomolecules in the same Figure 7.10 (a) and Figure 7.10 (b). In addition,

Figure 7.11 (a) and Figure 7.11 (b) show the plots of (I_{ON} and I_{ON}/I_{OFF} sensitivity) and (V_T and V_T sensitivity) for different dielectric constants of the biomolecules ranging from k= 3 to 12 with different values of negative charge densities of Q_{nf} = - 2x10^{11} cm^{-2}, - 6x10^{11} cm^{-2}, and -1x10^{12} cm^{-2}. Both sensitivities (I_{ON}/I_{OFF} sensitivity and S_{VT}) are getting increased with increase in dielectric constant, whereas I_{ON} is increased and V_T is decreased with the increased magnitude of the dielectric constant. Both sensitivities (I_{ON}/I_{OFF} sensitivity and S_{VT}) are getting increased with increase in dielectric constant, whereas I_{ON} current is increased and V_T is decreased with the increased magnitude of the dielectric constant.

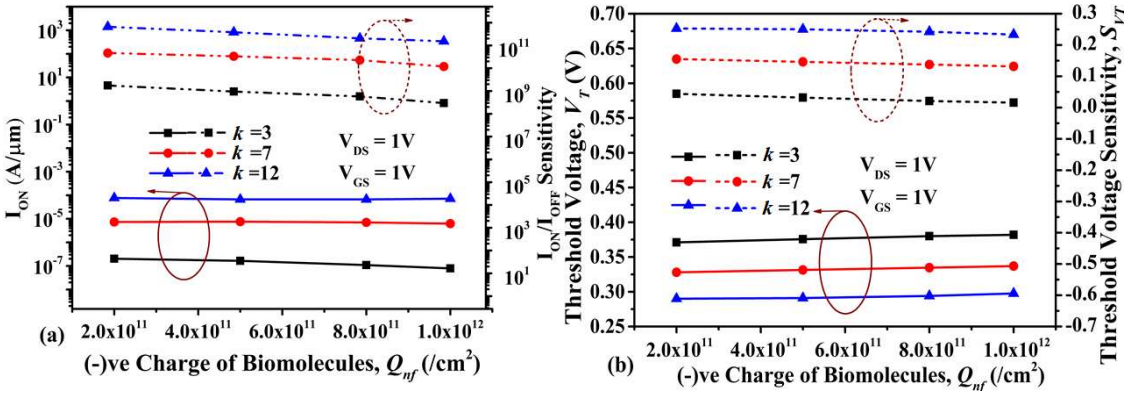

Figure 7.10 Plots of (a) I_{ON} and I_{ON}/I_{OFF} sensitivity and (b) Threshold voltage and threshold voltage sensitivity (S_{VT}) of DC-HJ-STFET based biosensor for different negative charged dielectric of biomolecules at V_{GS} = 1V, V_{DS} = 1.

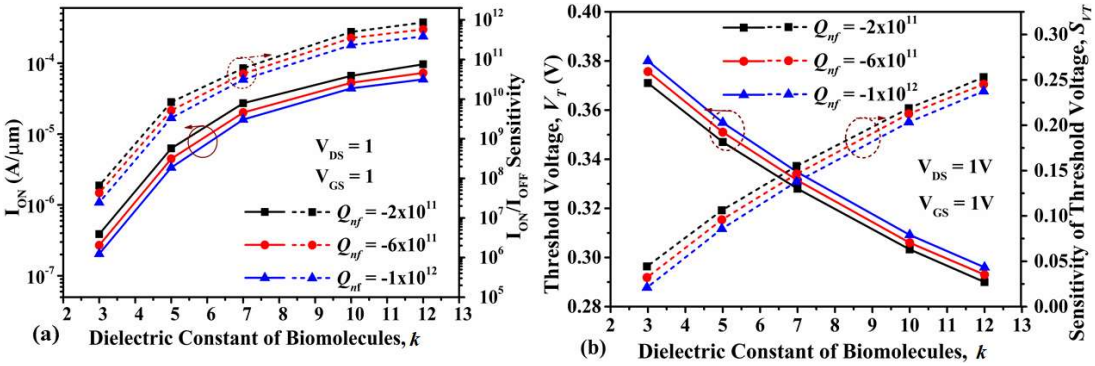

Figure 7.11. Plots of (a) I_{ON} and I_{ON}/I_{OFF} sensitivity and (b) threshold voltage and threshold voltage sensitivity of DC-HJ-STFET based biosensor for different dielectric constant of biomolecules at V_{GS} = 1V, V_{DS} = 1V.

7.4.4 Impact of Positive Charged Biomolecules

The I_{ON} current and I_{ON}/I_{OFF} sensitivities of DC-HJ-TFET based biosensor with the cavities filled with posititively charged biomolecules for k = 3, 7, and 12 are shown in Figure 7.12 (a) and Figure 7.12 (b), respectively. As demonstrated in Figure 7.12 (a) and Figure 7.12 (b), the magnitude of I_{ON} current , I_{ON}/I_{OFF} sensitivity, and V_T sensitivity increases as the positive charge value of the biomolecules increases, but V_T sensitivity. In addition, Figure 7.13 (a) and Figure 7.13 (b) shows the plots of (I_{ON} and I_{ON}/I_{OFF} sensitivity) and (V_T and S_{VT}) for different dielectric constants of the biomolecules ranging from k= 3 to 12 with different values of positive charge densities, such as Q_{nf}=$2x10^{11}$ cm^{-2}, $6x10^{11}$ cm^{-2}, and $1x10^{12}$ cm^{-2}. Table 7.4 summarizes various senstivity results discussed so far for the DC-HJ-TFET. As we have discussed previously, the ON-state current of biomolecules increases with positive charge density and decreases with negative charge density [233]. Hence, the sensitivity of the biosensors is also increased with positive charge density and decreased with negative charge density of the the biomolecules. The DC-HJ-STFET shows an I_{ON} sensitivity of $6.67x10^{12}$ which is two orders higher in magnitude than the recently reported biosensors [233]-[245].

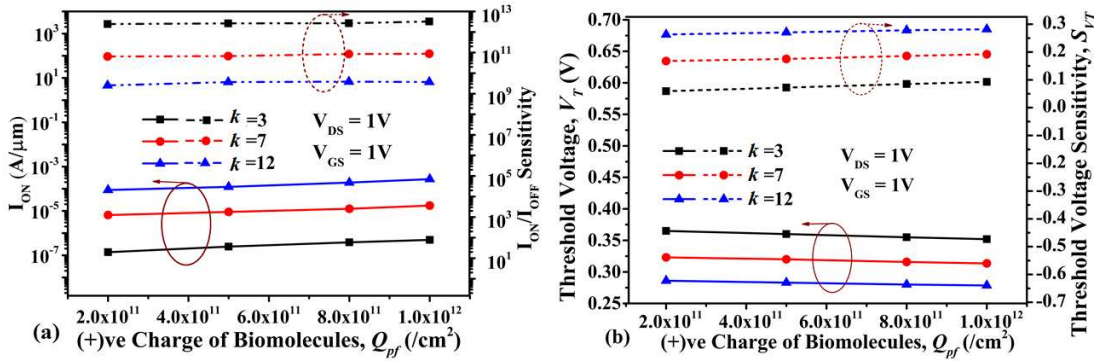

Figure 7.12 Plots of (a) I_{ON} and I_{ON}/I_{OFF} sensitivity and (b) threshold voltage and threshold voltage sensitivity of DC-HJ-STFET based biosensor for different positive charged dielectric of biomolecules at V_{GS} = 1V, V_{DS} = 1V.

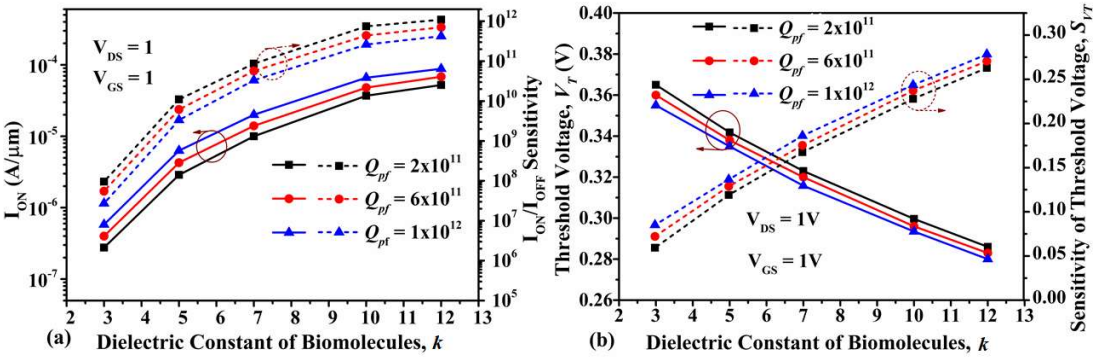

Figure 7.13 Plots of (a) I_{ON} and I_{ON}/I_{OFF} sensitivity and (b) threshold voltage (V_T) and threshold voltage sensitivity (S_{VT}) of DC-HJ-STFET based biosensor for different values of dielectric constant of biomolecules at V_{GS} = 1V, V_{DS} = 1V.

7.4.5 Effect of drain and back gate biasing

Figure 7.14 (a) depicts the drain current for various drain voltages. The device behavior has been altered from n-type TFET to p-type TFET for negative drain biasing. Figure 7.14 (b) depicts the device's transfer characteristics for various back gate voltages. It is interesting to note that the presence of back gate bias has no effect on the devices on state [248]. The ambipolar current, on the other hand, varies with the gate voltage. Ambipolar currents are similar for back gate voltages of 3 V and -3 V. Similar results can be obtained with back gate biases of 1 V and -1 V, though the difference in ambipolar currents is distinguishable. The ambipolar current decreases as the magnitude of the gate voltage decreases, therefore, I_{ON}/I_{OFF} sensitivity also decreases [248].

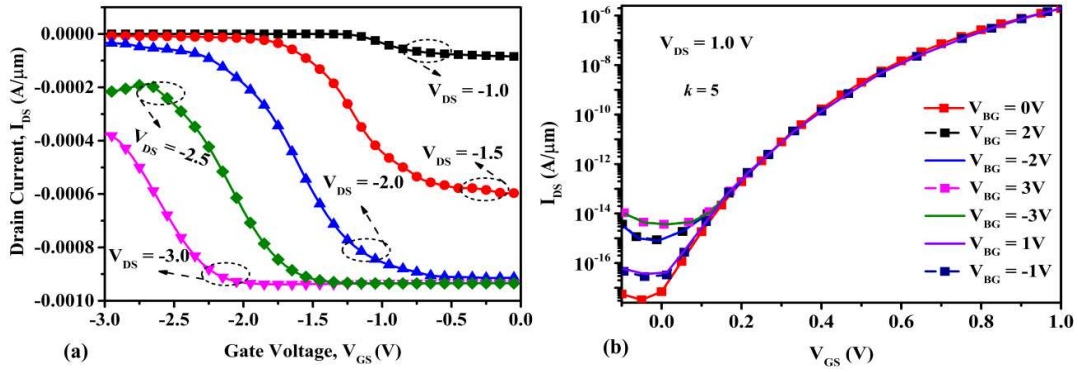

Figure 7.14 Plots of (a) drain current of DC-HJ-STFET based biosensor for different drain biasing (V_{DS}), and (b) I_D-V_{GS} characteristics of DC-HJ-STFET based biosensor for different V_{BG} (-3V to 3V).

Table 7.4 Proposed TFET Sensor (DC-HJ-STFET) Sensitivity for Neutral, (+)ve Charged and (-)ve Charged Biomolecules.

Biomolecules	Dielectric Constant	*Charge Density* (cm^{-2})	I_{ON}/I_{OFF} sensitivity	V_{th} sensitivity (S_{Vth})
Neutral Biomolecules	3	0	$1.0x10^{08}$	0.20
	5	0	$1.1x10^{10}$	0.21
	7	0	$1.3x10^{11}$	0.23
	10	0	$1.5x10^{11}$	0.26
	12	0	$1.0x10^{12}$	0.31
(+)*ve Charged Biomolecules*	12	$2x10^{11}$	$1.10x10^{12}$	0.32
	12	$4x10^{11}$	$1.11x10^{12}$	0.33
	12	$6x10^{11}$	$1.13x10^{12}$	0.34
	12	$8x10^{11}$	$1.15x10^{12}$	0.35
	12,	$1x10^{12}$	$1.20x10^{12}$	0.36
(-)*ve Charged Biomolecules*	12	$2x10^{11}$	$9.01x10^{11}$	0.19
	12	$4x10^{11}$	$8.80x10^{11}$	0.17
	12	$6x10^{11}$	$8.61x10^{11}$	0.16
	12	$8x10^{11}$	$8.40x10^{11}$	0.15
	12	$1x10^{12}$	$8.15x10^{11}$	0.13

7.4.6 Linearity Fit Verification

For the linearity fit analysis [249], authors have presented regression equation for the proposed device design and the response (linear) for the dielectric constant in the following ranges (a) k= 1 to k= 12 for three different charge density concentration values $2x10^{11}$ cm^{-2}, $6x10^{11}$ cm^{-2} and $1x10^{12}$ cm^{-2}, as shown in Fig. 15. The I_{ON}/I_{OFF} sensitivity follows good linearity with high correlation coefficient of 0.999 in lower dielectric constant values of biomolecules in region 1 shown in Figure 7.15 (a). On the other hand, the high dielectric constant follows relatively inferior correlation coefficient of .881 in region 2 as shown in Figure 7.15 (a). There are two different regression equations we

have presented, Eqn: 7.26 for lower dielectric constant ($1 \leq k \leq 4$) and Eqn: 7.27 for higher dielectric constant biomolecules ($4 < k \leq 12$).

$$y = 0.914x + 6.230 \tag{7.26}$$

$$y = 0.205x + 9.775 \tag{7.27}$$

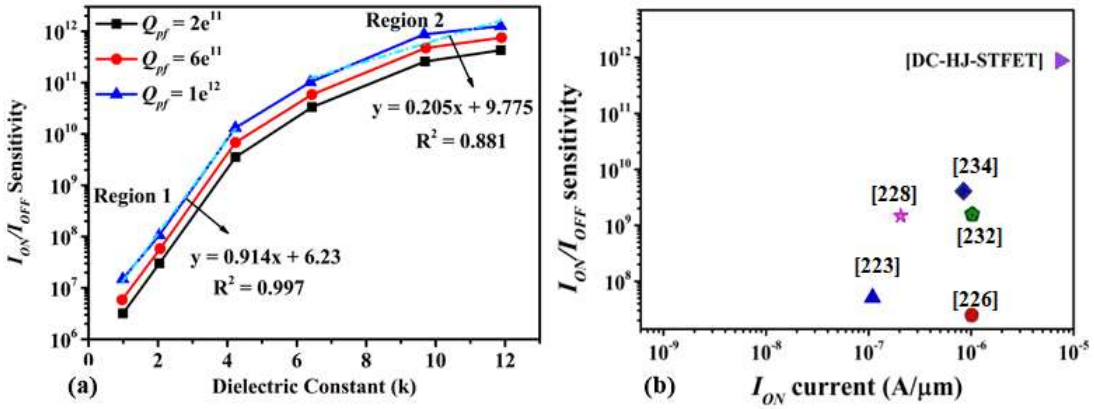

Figure 7.15 Plots of (a) Linearity fit of I_{ON}/I_{OFF} sensitivity vs. dielectric constant for (+)ve charged density biomolecules, and (b) Comparison of I_{ON}/I_{OFF} sensitivity of DC-HJ-STFET based biosensor with other TFETs.

7.4.7 Comparison With the Biosensor Based TFET

Figure 7.15 (b) shows the comparison metrics of I_{ON}/I_{OFF} sensitivity of DC-HJ-STFET based biosensor with the previously explored works on TFET based biosensors. However, the majority of biosensors are based on dielectric modulated phenomenon, which requires biomolecules to be introduced from both ends of the gate. Furthermore, because the type-II heterojunction (Gasb/GaAs) structure and introduction of SELBOX gap into the BOX, they provides the higher ON current and higher I_{ON} sensitivity than that of other devices [250]-[217], as shown in Table 7.5.

Table 7.5: I_{ON} and sensitivity comparison of DC-HJ-STFET biosensor with other reported TFET biosensors.

I_{ON}, and Sensitivity	This work	[250]	[251]	[234]	[217]
I_{ON}	7.9×10^{-5}	1.1×10^{-6}	1.2×10^{-8}	1.1×10^{-6}	2.1×10^{-6}
S_{Ion}	1.2×10^{12}	1.22×10^{8}	6.0×10^{6}	1.38×10^{5}	1.2×10^{4}
S_{VT}	0.37 V	------	------	1.2 V	------

7.4 Conclusions

A novel GaSb/GaAs HJ-STFET biosensor structure with optimized device dimensions has been presented in this paper. A stacked SiO_2/HfO_2 gate-oxide structure is used to improve the ON current of the proposed sensor. The ATLAS^{TM} TCAD has been used to analyse the performance parameters of the proposed biosensor. Biomolecules with varying dielectric constant (k) from 3 to 12 are assumed to be accommodated in the cavities created in the gate oxide of the HJ TFET. The impact of charge of biomolecules on the performance parameters of biosensor has been thoroughly investigated. The simulation results demonstrate that I_{ON} and I_{ON}/I_{OFF} sensitivity, and threshold voltage sensitivity (S_{Vth}) are improved with the increase in k values of the biomolecules. The negatively charged biomolecules lower the I_{ON}, I_{ON}/I_{OFF} sensitivity and also S_{Vth} sensitivity while reverse trends are observed for positively charged biomolecules. The sensitivity of the studied DC-HJ-STFET sensor is observed to be two orders higher in magnitude than the reported results. Further, we have observed, the I_{ON}/I_{OFF} sensitivity follows good linearity with high correlation coefficient in lower dielectric constant as compared to high dielectric constant biomolecules.